CORE
Metadata, citation and similar papers at core.ac.uk
Provided by Sheffield Hallam University Research Archive

SHARPENS YOUR THINKING

Transmission electron microscopy and x-ray diffraction investigation of the microstructure of nanoscale multilayer TiAlN/VN grown by unbalanced magnetron deposition

LUO, Q., LEWIS, D. B., HOVSEPIAN, P. E. and MUNZ, W. D.

Available from Sheffield Hallam University Research Archive (SHURA) at:

http://shura.shu.ac.uk/1134/

This document is the author deposited version. You are advised to consult the publisher's version if you wish to cite from it.

Published version

LUO, Q., LEWIS, D. B., HOVSEPIAN, P. E. and MUNZ, W. D. (2004). Transmission electron microscopy and x-ray diffraction investigation of the microstructure of nanoscale multilayer TiAlN/VN grown by unbalanced magnetron deposition. Journal of Materials Research, 19 (4), 1093-1104.

Repository use policy

Copyright © and Moral Rights for the papers on this site are retained by the individual authors and/or other copyright owners. Users may download and/or print one copy of any article(s) in SHURA to facilitate their private study or for non-commercial research. You may not engage in further distribution of the material or use it for any profit-making activities or any commercial gain.

Sheffield Hallam University Research Archive
http://shura.shu.ac.uk

Transmission electron microscopy and x-ray diffraction investigation of the microstructure of nanoscale multilayer TiAlN/VN grown by unbalanced magnetron deposition

Q. Luo*, D.B. Lewis, P.Eh. Hovsepian, W.–D. Münz

Materials Research Institute, Sheffield Hallam University, Sheffield, S1 1WB, UK.

Abstract: Cubic NaCl-B1 structured multilayers TiAlN/VN, having the bi-layer thickness ~3 nm and atomic ratios (Ti+Al)/V = 0.98 ~ 1.15 and Ti/V = 0.55 ~ 0.61 respectively, have been deposited by unbalanced magnetron sputtering at substrate bias voltages between -75 and -150V. In this paper, detailed transmission electron microscopy and X-ray diffraction revealed pronounced microstructure changes depending on the bias. At the bias -75V, the TiAlN/VN followed a layer growth model led by a strong (110) texture to form a T-type structure in the Thornton structure models, which resulted in a rough growth front, dense columnar structure with inter-column voids, and low compressive stress -3.3 GPa. At higher biases, the coatings showed typically a Type-II structure following the strain energy growth model, which were characterized by the columnar structure, void-free column boundaries, smooth surface, a predominant (111) texture, and high residual stresses between -7.9 and -11.7 GPa.

I INTRODUCTION

Nanoscale multilayer films of TiN/VN and TiN/NbN, epitaxially grown on single-crystal MgO(100) substrate by unbalanced magnetron (UBM) sputtering,[1] have shown super-high hardness values up to HV0.025 55 GPa. The super-hardness phenomenon was observed when the multilayer period λ falls into a specific range of a few nanometers. The micro-hardness, microstructure, and hardening mechanisms of the TiN/VN and TiN/NbN can be found in a series of publications, e.g., Refs. 2–5. The multilayers of TiN/NbN grown on a tool steel substrate achieved super-hardness values similar to single-crystal TiN/VN and TiN/NbN when the physical vapor deposition (PVD) conditions such as ion current, bias, and nitrogen partial pressure were optimized.[6,7] However, the films grown on steel substrate exhibited polycrystalline microstructure, which changed with the variation of deposition parameters. In particular, the highest hardness values were obtained when the films were grown at high bias voltage, e.g., −150 V.[6] Cross-sectional transmission electron microscopy (XTEM) of the TiN/NbN showed significant structure densification with increasing bias voltage.[7]

Following the pioneering work of the superhard TiN/VN and TiN/NbN, polycrystalline multilayer coating TiAlN/VN with a TiAlN-VN bi-layer thickness 3.5 nm has been grown on tool steel, which showed hardness values of $HK_{0.025}$ 33 GPa and HP_{50mN} of 39 GPa.[8] Whereas TiAlN is known for having oxidation resistance superior to that of TiN,[9] the incorporation of VN in the multilayer brought about a low friction coefficient (0.18– 0.4) and a low wear coefficient around 1.26×10^{-17} $m^3N^{-1}m^{-1}$. This is due to the formation of a lubricious vanadium oxide tribo-film on the worn surface.[10] Because of these properties, the TiAlN/VN has potential for applications as a wear-resistant coating, e.g., in cutting tools. However, the fundamental relationship between the deposition parameter and the microstructure should be understood before any successful tribological application can be made because microstructure plays a crucial role in determining the mechanical and tribological properties. For example, our previous research has revealed significant influence of substrate bias voltage (Ub) on the hardness and wear coefficient of TiAlN/VN.[8,11]

Microstructure of PVD coatings has attracted more and more research interest since the establishment of the well-known Thornton structure model.[12–14] Following the emergence of the UBM sputtering technique in later 1980s,[15] it has been reported that a negatively applied substrate bias voltage of Ub ≤ −200V is able to accelerate the ionized species so that dense coating of high hardness can be obtained,[16–19] although such dense coating is usually highly stressed.[16,17,20] In addition to the structure densification, the texture, or the preferred growth orientation,[11,21] has been another frequently addressed research issue, e.g., for transition metal nitride coatings with a B1-NaCl polycrystalline structure. For example, different textures such as (111), (110) and (100) can result, depending on the applied deposition parameters. Several models have been proposed to explain the textures, such as the surface energy model,[22–24] the strain energy model,[25] and other explanations based on the interaction between extrinsic dislocation loops and entrapped gaseous species.[26] These textures, however, were determined not only because of their important effect on the isotropic properties of coatings but also because x-ray diffraction (XRD) analysis is more

accessible than transmission electron microscopy, especially XTEM. Therefore, the texture models derived from XRD were rarely related to other microstructure features such as the nanoscale metallography, structural density, and surface roughness. The interrelationship between the texture and other major microstructure properties, as a function of the deposition parameters, should be understood in more detail, in particular for the newly developed nanoscale multilayers.

In this paper, XRD analyses and electron optics including plane-view and cross-sectional transmission electron microscopy (TEM) have been used to characterize the microstructure properties and texture development of UBM sputtered nanoscale multilayer TiAlN/VN grown under a series of substrate bias voltages between −75 and −150 V. The research has been emphasized in the variation of growth models that reflect different interrelations between the texture, residual stress, surface morphology, structure densification, and other cross sectional microstructure features of the coatings investigated. It has been found that the increase of substrate bias voltage from −75 to −150 V resulted in not only the progressive surface smoothening and structure densification, but also a transition of texture from (110) to (111). The different textures were derived from different growth models and thus were related to a variety of changes in the microstructure and the residual stresses. The results obtained provide a guide to explain the hardness and tribological properties of the TiAlN/VN coatings.

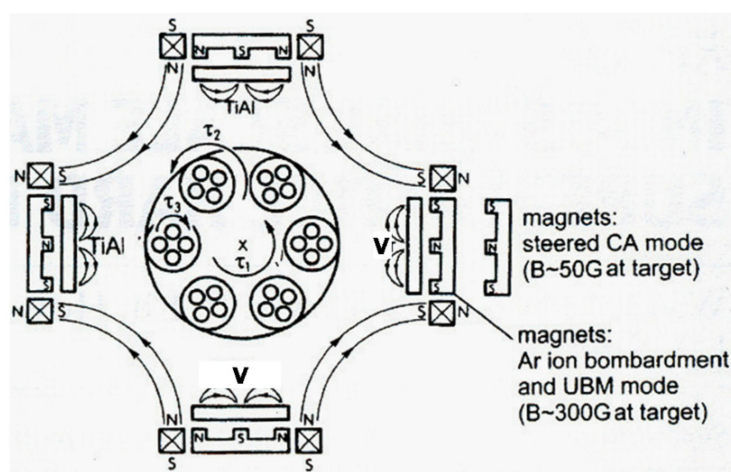

FIG. 1. Schematic diagram showing cross-section of the deposition chamber: two pairs of TiAl and V cathodes. Each cathode was equipped with an electro-magnetic coil and a permanent magnetron. It can be operated in both the steered cathodic arc mode for metal ion etching or evaporation and unbalanced magnetron mode for sputtering deposition.

II EXPERIMENTAL DETAILS

A. Deposition of TiAlN/VN coatings

A four-cathode Hauzer Techno Coatings (Venlo, The Netherlands) 1000-4 coater was used to deposit the TiAlN/VN coatings on pre-polished samples of stainless steel and cemented carbide material. The deposition chamber accommodated two pairs of rectangular cathodes of TiAl (atomic ratio Al/Ti = 1) and V (99.99% purity) (Fig. 1). Each of the cathodes can be operated either in a steered arc mode or in a UBM mode[27] In the middle of the chamber, the substrate samples were mounted on a three-fold rotating planetary turntable so that layered structure of the coatings was

achieved simply by sequential exposure of the sample surfaces to the vapor fluxes adjacent to the cathode pairs. A detailed process sequence and deposition parameters have been published elsewhere.[8,11,28] During the first stage of the process, a steered arc discharge was sustained on one of the V targets. The V^+ metal ion flux generated was accelerated towards the substrate surface by U_b = −1200 V. The metal ion bombardment is an effective method to obtain strong adhesion between the deposited coating and the substrate surface.[11,29] In the next stage a thin (0.3–0.5 μm) and low-stressed VN base layer was monolithically grown by UBM sputtering of the two V targets. Sputtering was carried out in a mixed N_2 and Ar atmosphere in total pressure control mode.[27] Following that, the four cathodes were operated in UBM mode simultaneously to grow TiAlN/VN multilayers. During this stage, one of the pre-selected substrate bias voltages between −75 and −150 V was applied for each batch. The final stage was the cooling down of the whole chamber till the temperature was below 200 °C.

B. Characterization of TiAlN/VN coatings

The coated stainless steel samples, which were ultrasonically cleaned, were characterized using an atomic force microscope (AFM) to determine the surface topography. The samples were also analyzed using the x-ray energy dispersive spectroscopy (EDS) in a scanning electron microscope (SEM) equipped with and Oxford Instruments (Bucks, UK) Links software system to determine the atomic ratios Ti/Al and Ti/V. Knoop hardness of the coatings, grown on cemented carbide substrate, was measured using a Mitituyo (Tokyo, Japan) MVK-H2 tester at an indenting load of 25 g.

X-ray diffraction analysis using Cu K_α radiation was undertaken to determine the crystalline structure, bi-layer thickness (low angle XRD), preferred texture and residual stress level of the TiAlN/VN coatings. The bi-layer thickness was also measured from high-resolution TEM images as well as from electron diffraction patterns obtained at large camera length (e.g. 6.4m). The texture factor T* was determined in accordance with the Harris inverse pole figure technique [30, 31] and was calculated from the following equation:

$$T^* = \frac{I_{(hkl)} / R_{(hkl)}}{\left(\frac{1}{n}\right)\sum_0^n I_{(hkl)} / R_{(hkl)}} \qquad (1)$$

where $I_{(hkl)}$ and $R_{(hkl)}$ are the intensities from the (hkl) reflections in the specimen and a random powder respectively and n is the number of reflections considered i.e. 7. Thus, a T* value of unity signifies a random orientation, whilst for T* values greater than unity the plane is considered to have a preferred orientation.

Glancing angle parallel beam geometry was used to determine the state of residual stress present in the coatings [32]. For cubic structures the lattice parameters, a_{hkl} (ψ) can be calculated for each diffraction peak where ψ is the angle between the diffraction vector of plane {hkl} and the normal to the film surface, such that ψ = θ - γ where θ is the Bragg angle and γ is the angle of

incidence of the x-ray beam relative to the specimen surface. For a thin film in a state of equi-biaxial stress the equation describing the stress dependence of the lattice parameter, a_ψ is related by the equation [33]:

$$a_\psi = \sigma\, a_0 \left\{ \left[{(1+\upsilon)}/{E} \right] \sin^2\psi - {2\upsilon}/{E} \right\} + a_0 \quad (2)$$

where a_0 is the unstressed lattice parameter, E is the elastic modulus and ν is the Poisson's ratio. For the Poisson's ratio, a value of 0.3 corresponding to that of TiN was used. The elastic modulus of each film was determined using a nano-indentation method. The stress can be determined from the slope of the least-squares fit of the plot of a_ψ versus $\sin^2\psi$ [33, 34]:

$$\sigma = \frac{Slope\ E}{a_0(1+\upsilon)} \quad (3)$$

Both plane-view and cross-section TEM foils were prepared. The coated steel sheets were sectioned using a high-speed silicon carbide disc saw under coolant. Then each sectioned piece was thinned following standard metallographic grinding and polishing to about 20 ~ 50μm thick. Final thinning to electron transparency was made in a precision ion polishing system (PIPS, Gatan, Munchen, Germany) using argon ions under 5 keV, 20 ~ 35 μA and incident angles ± 8°. The samples were thinned from both sides for the cross-section foils whereas the thinning was made only on the substrate side for the plane-view foils. A 200 kV Philips (Eindhoven, The Netherlands) CM-20 TEM instrument with a LaB_6 filament was used in the study.

III RESULTS

A. The surface morphology, composition, texture, hardness and residual stress of TiAlN/VN coatings

Figure 2 shows the surface morphology of TiAlN/VN coatings presented in AFM micrographs. The TiAlN/VN grown at U_b = −75 V showed a surface of submicron scale roughness. The cellular cells are believed to be the curved top of the TiAlN/VN columns. The boundaries of the cells formed a network of valleys which may arise from the so-called "shadow effect" during the sputtering growth. The TiAlN/VN coatings grown at higher U_b values showed smooth surfaces. In Fig. 2(b) and 2(c), the TiAlN/VN coatings grown at −95 and −125 V presented 2-dimensional equaxial cells, the morphology of which may indicate an erosion-like effect or surface bombardment resulting from the ion flux. However, the surfaces showed no evidence of the shadow effect.

Figure 3 shows quantitative EDS determination of atomic ratios Ti/Al, (Ti+Al)/V and Ti/V of the TiAlN/VN coatings as a function of U_b. The TiAlN/VN coating grown at U_b = -75V had a ratio Ti/Al = 1.01. Following the increase of substrate bias voltage, a linearly increased Ti/Al ratio was found, up to Ti/Al = 1.34 in the coating grown at U_b = -150V. The significant increase in the Ti/Al ratios is compared to the relatively stable ratios Ti/V, between 0.55 and 0.61, and (Ti+Al)/V, between 0.98 and 1.15. The EDS results indicate re-sputtering of metal atoms depending on the U_b. Considering the mass difference between Ti and Al, it is clear that preferential re-sputtering

occurred in relatively light element Al which led to a Ti-rich TiAlN component in the TiAlN/VN coatings grown at higher substrate bias voltages.

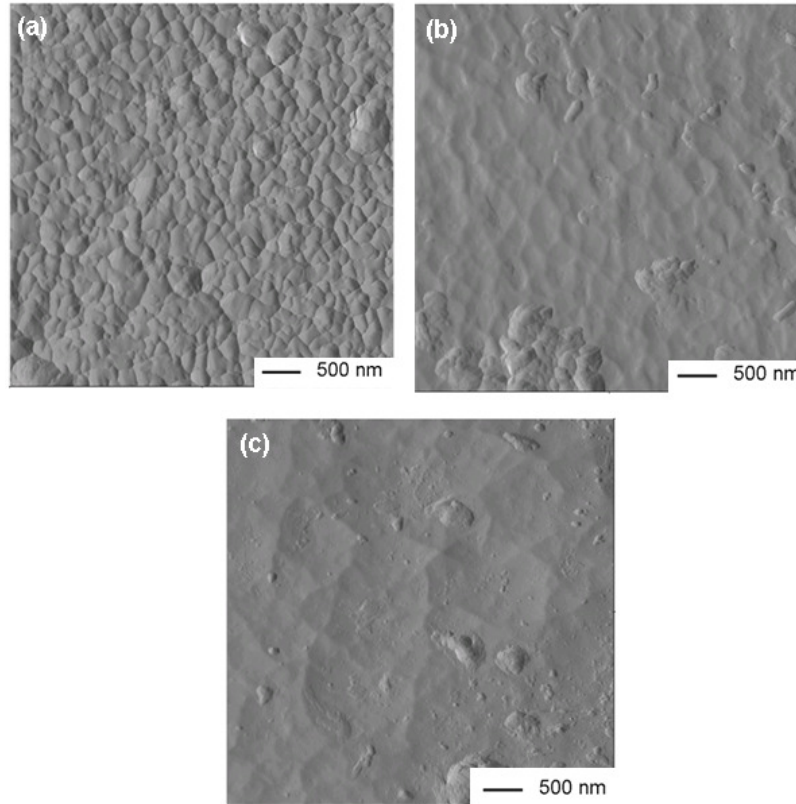

FIG 2 AFM micrographs showing the surface morphology of TiAlN/VN coatings grown at (a) U_b = -75V, (b) U_b = -95V, (c) U_b = -125V.

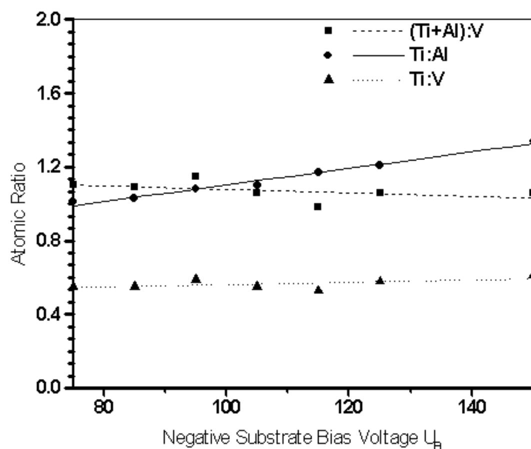

FIG 3 EDS-determined atomic ratios of the TiAlN/VN plotted against the variation of substrate bias voltage U_b between -75V and -150V.

From X-ray diffraction analysis, the TiAlN/VN coatings show a single phase of identical B1-NaCl structure but different preferred orientations depending on the U_b as illustrated in Figure 4. When U_b = -75V, a strong texture factor $T^*_{\{110\}}$= 4.2 was obtained compared to $T^*_{\{111\}}$= 1.5 and

extremely small value of $T^*_{\{100\}}$ respectively. This was the only case where the TiAlN/VN exhibits a strong {110} texture. However, when U_b was between -85 and -150V, $T^*_{\{111\}} \geq 6$ was the only identically strong texture factor whereas both the $T^*_{\{100\}}$ and $T^*_{\{110\}}$ were extremely low. The X-ray diffraction analysis suggests that, under the given deposition conditions, there exists a specific range of U_b above which the texture of TiAlN/VN coatings changes from (110) to (111).

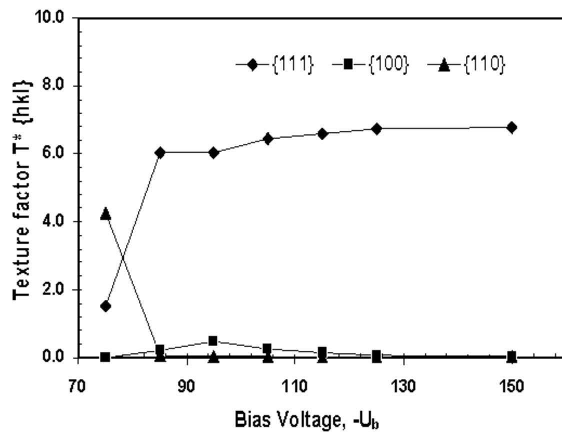

FIG 4 Texture factors $T^*_{\{100\}}$, $T^*_{\{110\}}$ and $T^*_{\{111\}}$ of TiAlN/VN coatings grown at substrate negative bias voltage between -75V and -150V.

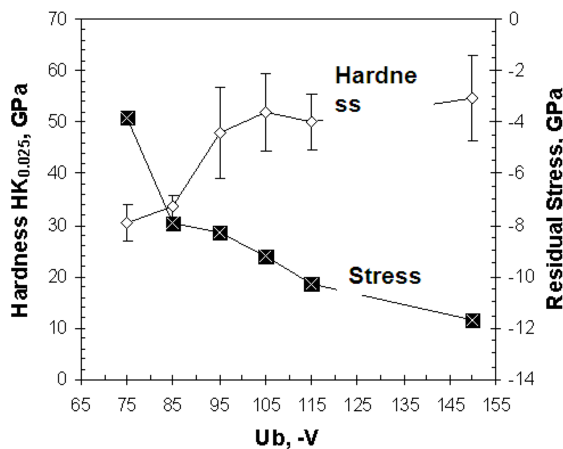

FIG 5 Residual compressive stress and hardness of TiAlN/VN coatings grown at different U_b between -75V and -150V.

Figure 5 plots the residual compressive stresses and hardness values against the variation in substrate bias voltage. The lowest residual stress −3.3 GPa was obtained in the TiAlN/VN coating grown at U_b = −75V. The TiAlN/VN coating grown at U_b = −75 V also showed the lowest hardness in the range of 30 GPa. However, the residual compressive stress increased from −3.3 to −7.9 GPa when the U_b was increased from −75 to −85 V. Further increase of the negative bias voltage leads to linear increase of stress from −7.9 to −11.7 GPa. In parallel, steady increase of hardness from 30 to 48 GPa was found corresponding to the increase of U_b from −75 to −95 V. Further increase of U_b to −150 V led to a hardness value of 55 GPa. Clearly the high hardness values were related to the increase of the residual compressive stresses. However, the pronounced effect on the hardness values were also derived from the microstructure changes.

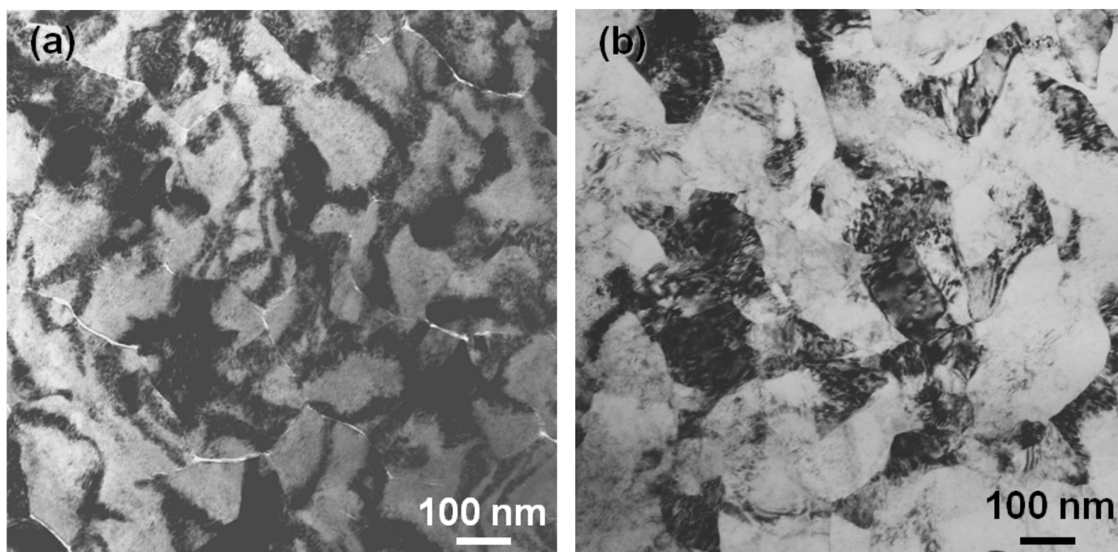

FIG 6 Plane-view TEM BF micrographs of TiAlN/VN grown at (a) U_b = -75V, (b) U_b = -95V.

B. The plane-view TEM and cross-sectional high-resolution TEM observations

Figure 6 shows plane-view TEM bright field (BF) micrographs of the TiAlN/VN coatings grown at U_b = −75 and −95 V. In Fig. 6(a), the TiAlN/VN (−75 V) exhibited two-dimentional (2D) equaxial blocks of grains having bright-contrasted low-density or void-presenting boundaries. The size of the grain blocks, in the submicron range, was constant to the cellular-like surface morphology presented in Fig. 2(a). The sub-dense boundary region was associated with the shadow effect mentioned above. Interestingly, it is noticed from the plane-view image that each grain block of the TiAlN/VN (−75 V) contained several subgrains rather than being a single crystal. This polycrystalline nature was also shown in the cross-sectional TEM BF images (to be shown later). The TiAlN/VN coating grown at higher U_b, e.g., −95 V, also exhibited 2D equaxial crystallines [Fig. 6(b)]. However, two significant differences between TiAlN/VN (−75 V) and TiAlN/VN (−95 V) can be found. TiAlN/VN (-95 V) showed completely dense-packed grain boundaries, associated with the smooth coating surface, i.e., no shadow effect [Fig. 2(b)]. Secondly, most of the grains shown in Fig. 6(b) were single crystalline with clearly defined grain boundaries, unlike the polycrystalline blocks in the TiAlN/VN (−75 V). Dislocation networks can be seen inside the structure, which might suggest ion bombardment induced lattice defects.

By imaging from defocused TEM BF mode, the multilayer substructure of the TiAlN/VN was observed (Fig. 7). The TiAlN and VN sublayers exhibited bright and dark contrast, respectively, due to the mass contrast mode.[2,4] In Fig. 7(a), the TiAlN/VN (−75 V) exhibits arch-like multilayer fringes. Distinct multilayer contrast, however, can be seen in the middle of each TiAlN/VN column. As the column boundary is approached, the multilayer fringes disappear, possibly as a result of low packing density or the overlapping between nearby subgrains. Figures 7(b) and 7(c) show that the multilayer fringes in the TiAlN/VN coatings grown at −95 and −125 V became more and more flat, and the column boundaries were well defined.

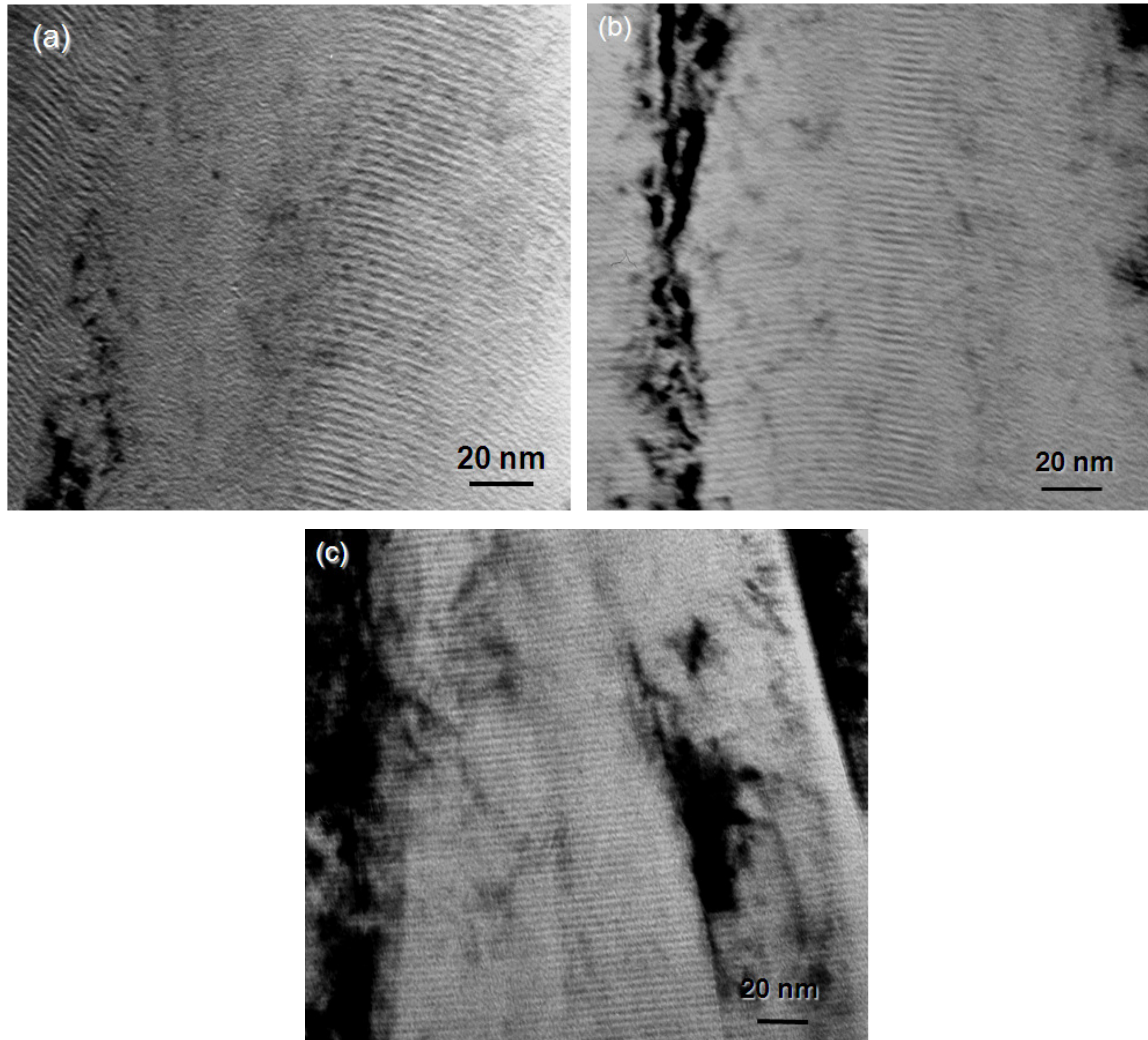

FIG 7 High resolution TEM-BF micrographs showing the TiAlN and VN multilayer fringes in the TiAlN/VN coatings grown at (a) U_b = -75V, (b) U_b = -95V, (c) U_b = -125V.

The increase of substrate bias voltage showed a weak effect on the bi-layer thickness of the TiAlN/VN coatings. The bi-layer thickness was measured not only from the high-resolution images like those in Fig. 7, but also from low-angle XRD and TEM electron diffraction. The results are plotted in Fig. 8 against the increase of U_b. The bi-layer thickness of the TiAlN/VN fell in a range between 3.05 and 3.3 nm. Despite the data scattering arising from the different calibrations of the TEM and XRD techniques, a weak trend suggested that high bias voltage resulted in slightly smaller bi-layer thickness due to the increased intensity of ion bombardment. As the U_b was increased from −75 to −150 V, the bi-layer thickness was decreased by approximately 5%.

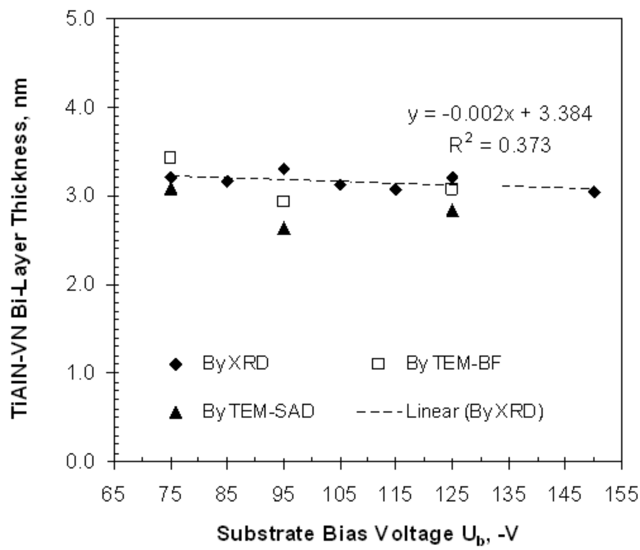

FIG 8 Bi-layer thickness of the TiAlN/VN multilayers plotted against the variation of substrate bias voltage U_b between -75V and -150V.

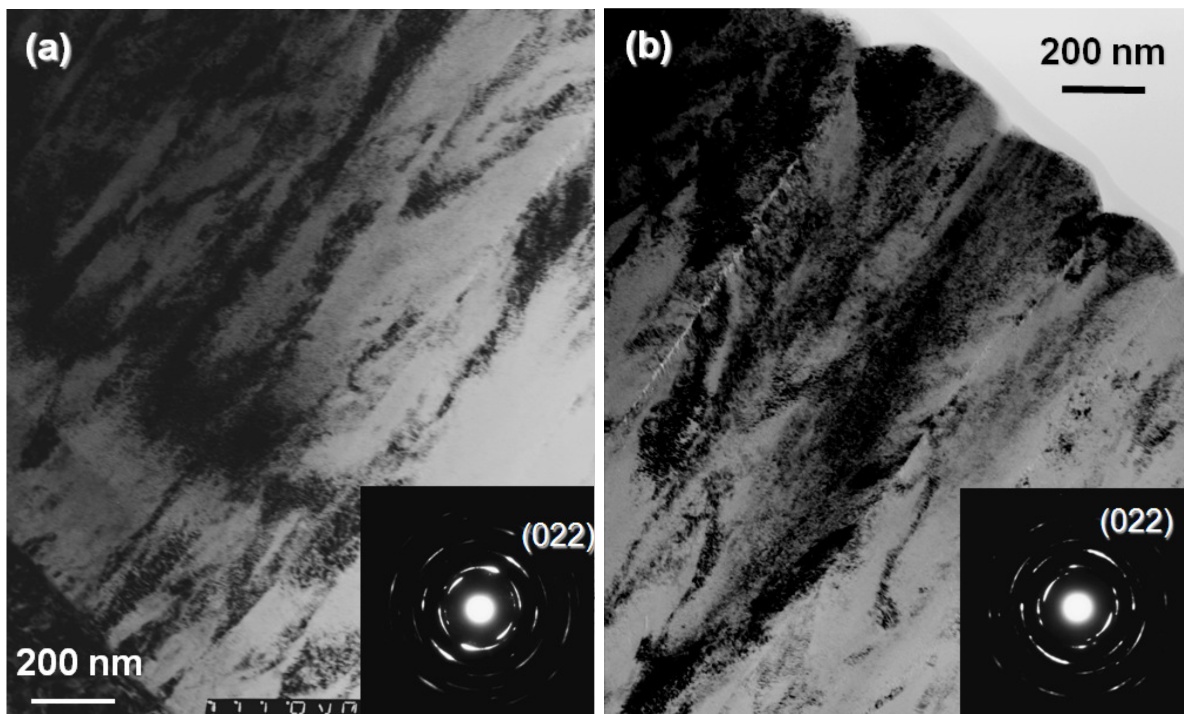

FIG 9 Cross-section TEM micrographs and associated SAED patterns obtained from (a) the lower and (b) upper parts of the TiAlN/VN grown at -75V.

C. Growth models observed by cross-sectional TEM

In Fig. 9, cross-sectional TEM BF micrographs show the columnar microstructure of TiAlN/VN grown at −75 V. The coating exhibited a T-type structure according to the Thornton's structure

model,[12,14] i.e., a transition structure zone between the fibrous and porous structure (Type-I) and the columnar and dense structure (Type-II). In the lower part, initial TiAlN/VN was grown from the fine columns of VN base layer. At the transition from VN to TiAlN/VN, a region of microstrain was observed, possibly due to the local mismatch between the VN and TiAlN/VN. The column width of the TiAlN/VN in the initial growth was around 50–150 nm [Fig. 9(a)]. Following that, V-shape columns were associated with coarse columns which, when approached the surface, became no less than 300 nm. Voids or low-density areas were clearly imaged at the column boundaries [Fig. 9(b)]. The curved top of the columns together with the inter-column voids, which were typically seen for magnetron sputtered coatings,[6,8,16,19,29] agreed well with the AFM and plane-view TEM results.

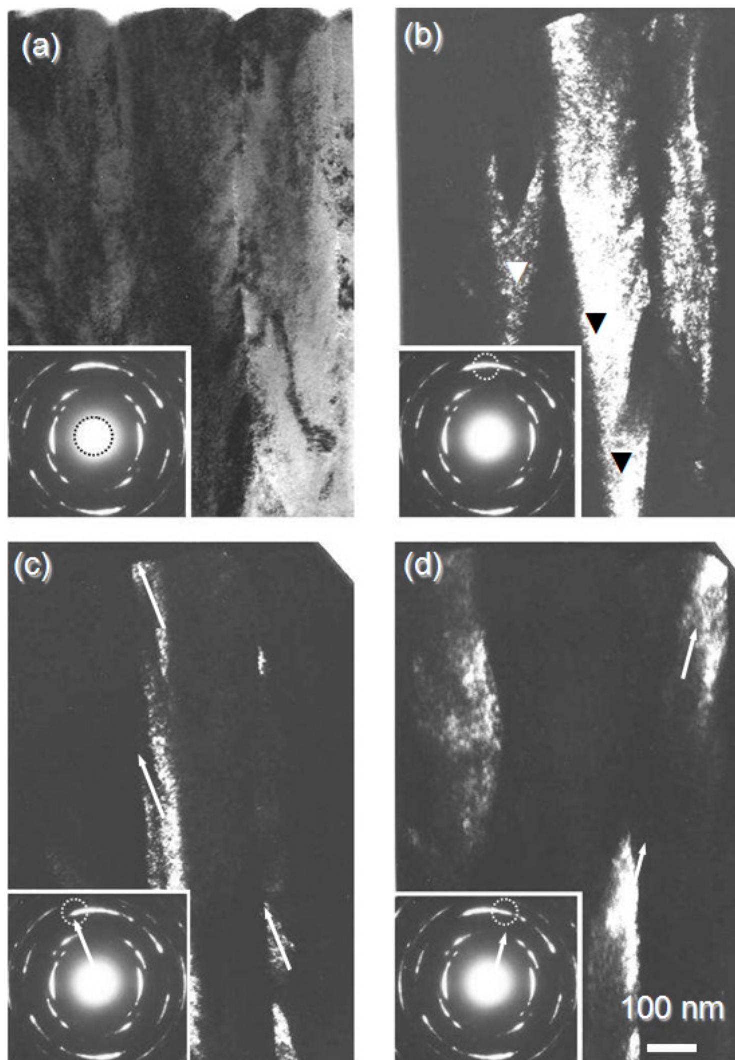

FIG 10 Orientation of TiAlN/VN columns determined by SAED and central DF imaging. The diffraction beam used for imaging is circulated in each inserted SAED pattern.
(a) A BF image with associated SAED pattern taken from the upper part of Figure 9b.
(b) A DF image indicating that majority of (110) textured TiAlN/VN columns being aligned to the column axis.
(c and d) DF images showing sub-grains each having the (110) texture depending on the local growth curvature.

The inserted selected area electron diffraction (SAED) patterns in Fig. 9 indicate that the TiAlN/VN grown at −75 V exhibited a strong (110) texture. Moreover, the SAED pattern taken in the lower part of the TiAlN/VN [Fig. 9(a)] showed concentrated (022) diffraction arcs, which was compared to the strong angular spread of the (022) arcs obtained in the middle and upper part of

the coating. Therefore, it is suggested that the fine columnar grains in the low part exhibited a concentrated (110) texture well aligned to the growth direction. Then in the middle and upper parts, the angular spread suggested that some of the (110) oriented subgrains were misaligned to the column axis. Such distribution of subgrains is also seen by plane-view TEM in Fig. 6(a), in which each coarse block comprised a number of subgrains.

The locally misaligned growth orientation in the TiAlN/VN (−75 V) columns has been confirmed by TEM dark field (DF) imaging, shown in Fig. 10. Figure 10(a) is a reference BF image. For Figs. 10(b)–10(d), the DF images were taken by locating the objective aperture at different places of the {022} diffraction arc (indicated in each inserted SAED): (b) At the central part of the {022} arc along the growth direction to illuminate those subgrains aligned to the column axis, (c) at left hand side of the {022} arc to illuminate the subgrains counter-clockwise aligned to the column axis, (d) at right hand side of the {022} arc to illuminate the subgrains clockwise aligned to the column axis.

Figure 10(b) shows that the central part of each TiAlN/VN column had its (110) plane parallel to the local growth front. Re-nucleations were observed in the columns as indicated in the V-shape regions. However, the inter-column regions did not have its (110) plane aligned to the column axis. Instead, Figs. 10(c) and 10(d) show that the local (110) plane was aligned to the arch-like curvature (arrowed respectively). In brief, the TEM DF images confirmed that, TiAlN/VN (−75 V) exhibited such a (110)-textured layer growth model in which (110) was the leading growth plane not only in the central part of each TiAlN/VN column but also in the curved boundary region.

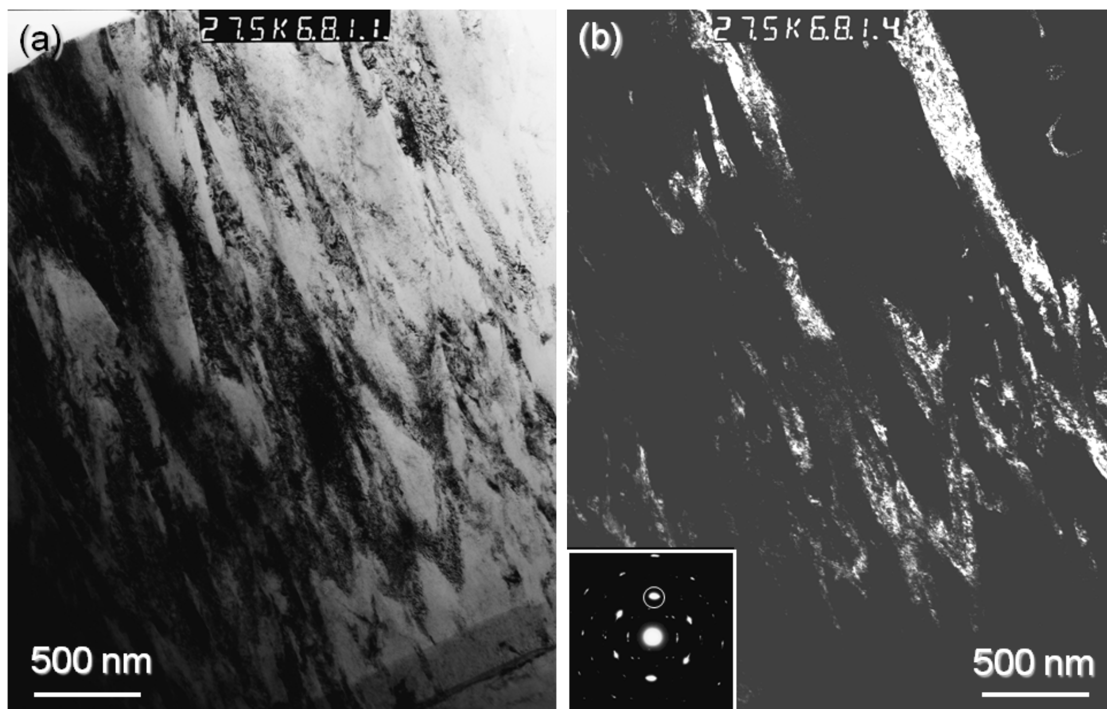

FIG 11 Cross-sectional (a) BF and (b) DF micrographs of TiAlN/VN coating grown at -95V, showing competitive columnar growth, void-free structure densification, and the smooth coating surface.

Figures 11(a) and 11(b) present a pair of cross sectional TEM BF and DF micrographs of the TiAlN/VN grown at U_b = −95 V. V-shape irregular grains of fully dense-packing density developed during the lower part of the TiAlN/VN (−95 V) indicative of competitive column growth. The competitive growth was also evidenced by that each TiAlN/VN column was a single crystalline, which was in contrast to the polycrystalline TiAlN/VN (−75 V) columns in Fig. 9. The TiAlN/VN (−95 V) was absolutely dense-packed without any inter-column void. Such completely void-free structure was also presented in TiAlN/VN (−85 V). Figures 12(a) and 12(b) show the TEM BF and DF micrographs of the TiAlN/VN coating grown at U_b = −125 V. Similar to the TiAlN/VN (−95 V), the coating again exhibited, in the lower part, coarse and interrupted columnar grains with some of them having V-shape morphology indicative of competitive growth. The TiAlN/VN was also completely void-free, which was compared to the presence of voids in the VN base layer where the VN was grown at U_b = −75 V. In the upper part of the TiAlN/VN (−125 V), a smooth coating surface is seen with typical columnar grains and void-free column boundaries (Fig. 13). The multilayer fringes are flat across the imaged TiAlN/VN columns.

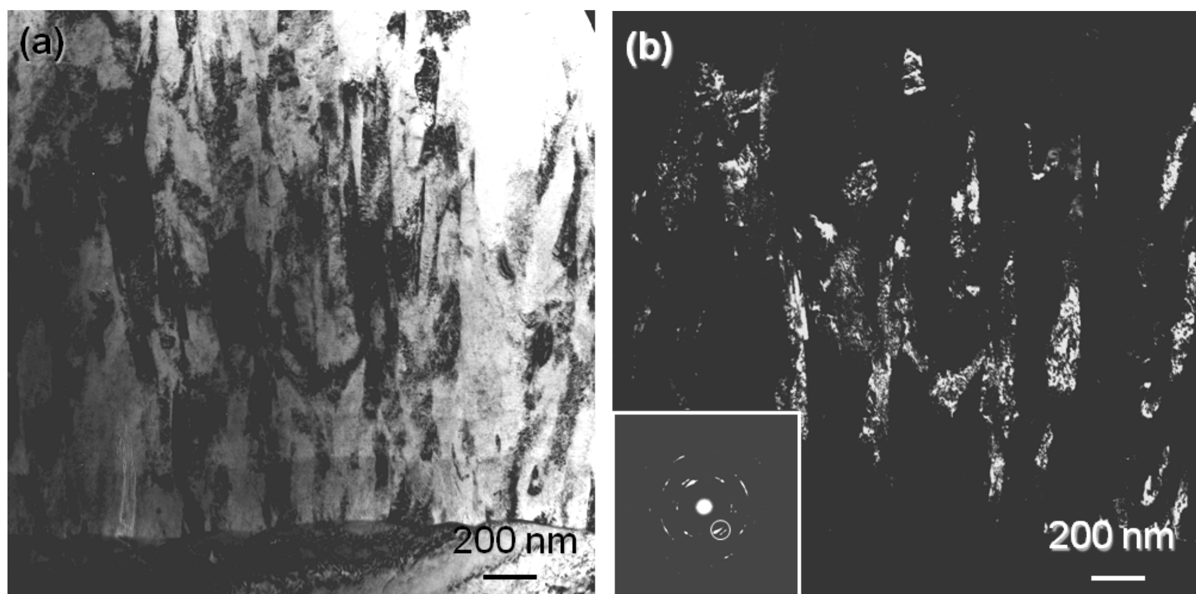

FIG 12 Cross-sectional (a) BF and (b) DF micrographs of TiAlN/VN coating grown at -125V, showing competitive growth and coarsening of void-free columns.

IV DISCUSSIONS

A. Microstructure of TiAlN/VN at U_b = -75V

Nanostructured multilayer TiAlN/VN coatings with bi-layer thickness in the range of 3 nm have been grown using the multi-target UBM sputtering process. The results presented show that the substrate bias voltage has pronounced effect on the microstructure of the deposited coatings. The TiAlN/VN grown at U_b = −75 V exhibited a T-type structure according to the Thornton's

structure model.[12,14] This classification was supported by the presence of coarse polycrystalline columns (Fig. 9) and the rough growing surface [Figs. 2(a), 7(a), and 9(a)]. Whereas the coating was predominantly dense, the rough surface resulted in a shadow effect during the coating growth and consequently the formation of inter-column voids [Figs. 6(a) and 9(a)]. This phenomenon was reported elsewhere in similar cases of sputtering deposition under low U_b.[17,19,20]

FIG 13 A cross-sectional BF micrograph showing flat multilayer fringes, smooth surface and completely void-free columnar structure in the TiAlN/VN (-125V).

A similar T-type structure has also been presented in other magnetron (or UBM) sputtered nitride coatings, such as monolithically grown coating TiN[16,19] and multilayer coatings TiN/NbN,[6] TiAlN/TiNbN,[29] and CrN/NbN.[8] The dense structure of the TiAlN/VN coating was attributed to the unbalanced magnetron mode and to the applied bias voltage −75 V, as it has been reported that sputtered coatings TiN and TiAlN grown at U_b = 0 showed corn-like columns with open column boundaries.[19] According to reports,[17,18] structure densification can be achieved in the UBM sputtering mode either by increasing ion ionization, e.g., with J_i/J_{me} = 1 to 7, or by increasing ion energy when a low negative substrate bias is applied. For example, fully dense structure of magnetron sputtered TiN/NbN multilayers has been reported depending strongly on the applied substrate bias voltage at U_b = −(80 to 150) V.[6,7]

Both the XRD and XTEM analyses revealed the strong (110) texture developed in the TiAlN/VN (−75 V) (Figs. 4 and 9). The (110) texture was related to the polycrystalline characteristic of the TiAlN/VN columns which led to a (110) textured layer growth model (Fig. 10). The (110) texture was similarly found in other magnetron sputtered coatings like TiAlN/CrN,[11] CrN,[21] and VN.[35] In magnetron sputtered -$VN_{0.9}$, for example, a (110) texture was observed when the substrate bias voltage was between −50 and −80 V.[35] In literature, a surface energy model was proposed to explain the layer growth in column-like structured nitride coatings.[22–24] This proposed model, however, was applied only to the coatings which show a (100) texture because the {100} planes have the highest density of atoms in the B1-NaCl structure. Thus, the growth model in the TiAlN/VN (−75 V) could not be explained using the lowest surface energy model. Perry and co-authors proposed a model to explain the (110) texture that a tetrahedrally located dumb-bell nitrogen pair

along the [220] direction of the NaCl-B1 lattice, e.g., in TiN, favors the development of (110) texture.[26] Should this model be valid, a consequence of the preferential interstitial nitrogen distribution would be the expanded d-spacing and enhanced distortion of the (220) plane perpendicular to the growth direction. This has been confirmed in our previous XRD work on UBM sputtered TiAlN/CrN[36] and CrN,[21] where both exceptionally large d-spacing and expanded line broadening have been shown.

B. Microstructure of TiAlN/VN at $U_b \geq -85V$

TiAlN/VN coatings grown at substrate bias voltages between −85 and −150 V showed smooth surfaces, completely dense and columnar structure, and a strong (111) texture. The smooth surfaces have been demonstrated by the presented AFM and cross-sectional TEM micrographs (Figs. 2, 7, and 13). The coatings exhibited typically columnar morphology along the growth direction (Figs. 11−13) and in plane-view equaxial granular structure [Fig. 6(b)]. The columnar grains contained high density dislocation network indicative of ion bombardment induced lattice defects. Such microstructure can be fitted into the II-type structure in the Thornton model.[12–14] The increased ion bombardment following the increase of the bias voltage resulted in re-sputtering on the growing film, preferentially aluminum atoms, which led to the increase of the Ti/Al ratio (Fig. 3) and the decrease of the bi-layer thickness (Fig. 8). These results were generally consistent with literatures.[11,12,14–16] However, the TiAlN/VN coatings maintained a constant Ti/V ratio and only a marginal decrease of the (Ti+Al)/V ratio within the given range of U_b (Fig. 3). The bi-layer thickness of the TiAlN/VN was maintained between 3.05 and 3.3 nm (Fig. 8).

The TiAlN/VN coatings grown at Ub between −85 and −150 V exhibited an identical (111) texture (Fig. 4) and high compressive stresses (Fig. 5). The correlation between the (111) texture and the high residual stress can be explained using the strain energy model.[25] TiN-type coatings were reported to have the lowest strain energy if the growth was along the ⟨111⟩ direction.[23–25] In this model, the lowest strain energy becomes the major driving force in determining the preferred growth orientation of highly strained coatings. Other researchers suggested (111) to be a thermodynamically favorable texture because it was found that the entrapped argon and nitrogen in high-biased coatings segregated along the extrinsic dislocation loops embedded in the (111) plane.[21] Associated with this explanation, our plane-view TEM micrograph [Fig. 6(b)] revealed the presence of high-density dislocations.

C. Hardness of TiAlN/VN coatings

The TiAlN/VN coatings deposited on cemented carbide substrate showed hardness values between 30 and 55 GPa depending on the applied U_b (Fig. 5). The coatings deposited at −75 and −85 V showed relatively lower hardness, 30 and 34 GPa respectively. The hardness increased steeply to 48 GPa at U_b = −95 V, followed by slower increase to 55 GPa with the increase of U_b up to −150 V.

The relatively lower hardness in the TiAlN/VN (−75 V) indicates that the low-density or sub-dense column boundaries [shown in Figs. 6(a) and 9] result in lower hardness of polycrystalline multilayer coating. Similar influence of porosity on hardness was also seen in other polycrystalline multilayer coatings TiN/VN and TiN/NbN.[6,7] The sub-dense structure, however, also led to low residual stress, which is believed to be beneficial to the wear resistance of the TiAlN/VN.[8,11] It has been found that the TiAlN/VN (−75 V) showed much lower sliding wear coefficient than others grown at higher Ub. Similar cases were also reported in other multilayer coatings CrN/NbN and TiAlN/CrN.[8,11] Previous wear mechanism study has revealed both spalling and delamination wear in nanostructured coatings TiAlN/CrN and TiAlCrYN.[37] Low compressive stress in the TiAlN/VN (−75 V) would reduce the tendency of these wear modes.

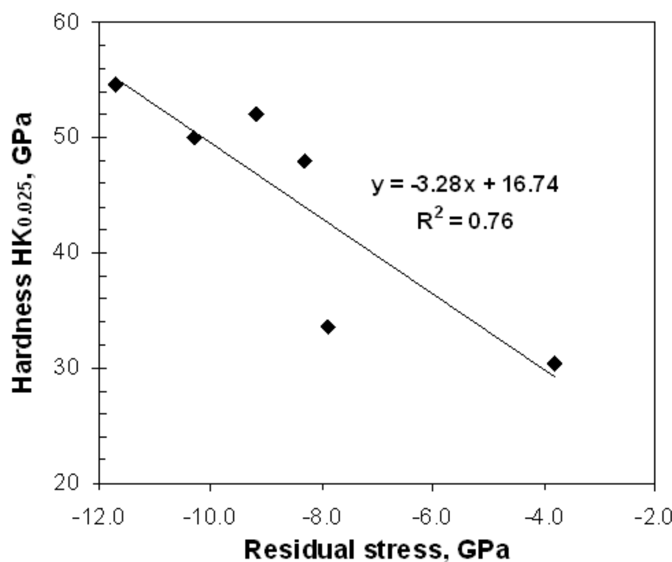

FIG 14 Correlation between hardness and residual stress of TiAlN/VN coatings.

The high hardness values of the TiAlN/VN coatings grown at U_b from −95 to −150 V were related to the high compressive stresses. The hardness values presented in Fig. 5 are plotted against the associated residual stresses in Fig. 14, indicating approximately linear increase of hardness with increase stress. It has been known that the hardness values measured by indentation reflect not only the intrinsic hardness of the materials themselves but also the resistance from the compressive stresses. In magnetron sputtered TiAlN and TiN coatings, the [N]/[Ti+Al] and [N]/[Ti] ratios increase with increasing ion energy.[17] Furthermore, the high hardness values were related to the microstructure changes in the TiAlN/VN coatings. TEM observations have also found high density lattice defects in the high-biased coatings, i.e., dislocations [Fig. 6(b)]. In literature, extrinsic dislocation loops and entrapped Ar were reported to generate at high bias voltages.[21]

In summary, the substrate bias voltage has shown significant influence on the multilayer coatings TiAlN/VN for the surface morphology, structure densification, texture, residual stress, and hardness. The microstructure changes have been found to derive from the growth model change

from (110) textured layer growth to (111) textured competitive columnar growth. Further research is expected to find detailed friction and wear properties of the coatings.

V CONCLUSIONS

By multi-target unbalanced magnetron sputtering deposition, nanoscale multilayer TiAlN/VN coatings having bi-layer thickness approximately 3 nm have been grown. Though they have an identical cubic B1-NaCl crystallographic structure, the coatings show different structure densification and growth models as well as residual stresses depending on the applied substrate bias voltages between −75 and −150 V. A (110) textured layer growth model is proposed for the TiAlN/VN grown at −75 V. At −75 V, the TiAlN/VN coating showed a strong (110) texture, densely packed columnar structure and inter-column voids. The column size increased with coating thickness which leads to a polycrystalline nature in each column. In particular, the low scale of residual stress (−3.8 GPa) was associated with the sub-dense column boundaries. This coating belonged typically to the T-type structure in the Thornton structure model. Completely void-free TiAlN/VN coatings grown at U_b =−85 V showed high residual stress of −8 GPa and a strong (111) texture. Further increase in the bias voltage led to an enhanced (111) texture and a linear increase in the residual stress from −8 to −11.7 GPa. The identical (111) texture in the highly stressed coatings was developed by competitive columnar growth following the lowest strain energy model. The increase of substrate bias voltage also eliminated the surface roughening of the TiAlN/VN coatings leading to a smooth coating surface.

ACKNOWLEDGEMENTS

The authors acknowledge partial financial support by European Community through the project ‘Revolutionary New Steels, Coated and Designed for Cutting Tools to Machine Aluminium and Titanium Alloys’ (No. GRD1-2001-40514). The authors wish to thank Dr. Xiaoxue An for the help in AFM messurement.

REFERENCES

1. U. Helmersson, S. Todorova, S.A. Barnett, J.E. Sundgren, L.C. Market, J.E. Greene, J. Appl. Phys. **62**, 481 (1987).
2. M. Shinn, L. Hultman, S.A. Barnett, J. Mater. Res. **7,** 901 (1992).
3 P. B. Mirkarimi, S. A. Barnett, K. M. Hubbard,T. R. Jervis, L. Hultman, J. Mater. Res. **9**, 1456 (1994).
4 L. Hultman, L. R. Wallenberg, M. Shinn, S.A. Barnett, J. Vac. Sci. Technol. **A10,** 1618 (1992).
5 S.A. Barnett, M. Shinn, Annu. Rev. Mater. Sci. **24,** 481 (1994).
6 X. Chu, M.S. Wong, W.D. Sproul, S.L. Rohde, S.A. Barnett, J. Vac. Sci. Technol., **A14**, 2500 (1999).
7 X. Chu, M.S. Wong, W.D. Sproul, S.A. Barnett, J. Mater. Res. **9**, 1456 (1994).
8 P.Eh.Hovsepian, D.B.Lewis, W.-D. Münz, Surf. Coat. Technol. **133-134,** 166 (2000).

9 K. Noguchi, N. Kitagawa, H. Ohara, H. Animoto, Proceedings of 1st French & German Conf. on High Speed Machining, University of Metz, June 1997, 407 (1997).
10 C.P. Constable, J. Yarwood, P.Eh. Hovsepian, L.A. Donohue, D.B. Lewis, W.-D. Münz, J. Vac. Sci. Technol. **18A,** 1681 (2000).
11 W.-D. Münz, D.B. Lewis, P.Eh. Hovsepian, C.Schönjahn, A. Ehiasarian, I.J. Smith, Surf. Eng. **17**, 15 (2001).
12 J.A.Thornton, J. Vac. Sci. Technol., **11,** 666 (1974).
13 R. Messier, A.P. Giri, R.A. Roy, J. Vac. Sci. Technol. **A2**, 500 (1984).
14 C.R.M. Grovenor, H.T.G. Hentzell, D.A. Smith, Acta Metall. **32**, 773 (1984).
15 B. Window, N. Savvides, J. Vac. Sci. Technol. **A4**, 196 (1986).
16 W.-D. Münz, Surf. Coat. Technol. **48**, 81 (1991).
17 F. Adibi, I.Petrov, J.E. Greene, L.Hultman, J.E.Sundgren, J. Appl. Phys. **73**, 8580 (1993).
18 J.E. Yehoda, B. Yang, K. Vedam, R. Messier, J. Vac. Sci. Technol. **A6**, 1631 (1988).
19 L. Hultman, W.-D. Münz, J. Musil, S. Kadlec, I. Petrov, J.E. Greene, J. Vac. Sci. Technol. **A9**, 434 (1991).
20 I. Petrov, F. Adibi, J.E. Greene, L. Hultman, J.-E. Sundgren, Appl. Phys. Lett. **63**, 36 (1993).
21 T. Hurkmans, D.B. Lewis, H. Pariton, J.S. Brooks, W.D. Münz, Surf. Coat. Technol. **114,** 52 (1999).
22 C. M. Cotell, J. K. Hirvonen, Surf. Coat. Technol. **81**, 118 (1996).
23 G. Knuyt, C. Quaeyhaegens, J. DHaen, L.M. Stals, Surf. Coat. Technol. **76**, 311 (1995).
24 G. Knuyt, C. Quaeyhaegens, J. DHaen, L.M. Stals, Thin Solid Films **258**, 159 (1995).
25 U.C. Oh, J.H. Je, J. Appl. Phys. **74**, 1692 (1993).
26 A.J. Perry, V. Valvoda, D. Rafaja, Vacuum **45**, 11 (1994).
27 W.-D. Münz, D. Schulze and F. Hauzer, Surf. Coat. Technol. **50**, 169 (1992).
28 L. A. Donohue, W.-D. Münz, D. B. Lewis, J. Cawley, T. Hurkmans, T. Trinh, I. Petrov, J. E. Greene. , Surf. Coat. Technol. **93**, 69 (1997).
29 I Petrov, P. Losbichler, D. Bergstrom, J. E. Greene, W.-D. Münz, T. Hurkmans, T. Trinh, Thin Solid Films, **302**, 179 (1997).
30 G. B. Harris Phil. Mag., **43**, 113 (1952).
31 D. S. Rickerby, A. M. Jones, B. A. Bellamy, Surf. Coat. Technol. **37**, 111 (1989).
32 D. E. Geist, A. J. Perry, J. R. Treglio, V. Valvoda, and D. Rafaja, Adv. X-ray Analysis, **38**, 471 (1995).
33 V. Valvoda, A. J. Perry, L. Hultman, J. Musil S. Kadlec, Surf. Coat. Technol. **49**, 181 (1991).
34 A. J. Perry, Thin Solid Films, **193-194**, 463 (1990).
35 G. Farges, E. Beauprez, M.C. Staine Catherine, Surf. Coat. Technol. **54-55**, 115 (1992).
36 D.B. Lewis, I.P.Wadsworth, W.-D. Münz, R. Kuzel Jr., V. Valvoda, Surf. Coat. Technol., **116-119**, 284 (1999).
37 Q. Luo, W. M. Rainforth, W.-D. Münz, Wear **225-229,** 74 (1999).
38 Q. Luo, W. M. Rainforth, W.-D. Münz, Scripta Materialia, **45**, 399 (2001).